# VLF Waveguide Propagation: The Basics

Kenneth J.W. Lynn

*Ionospheric Systems Research, 16 Heritage Dr., Noosaville 4566, Australia*

**Abstract.** In recent times, research has moved towards using VLF radio transmissions propagating in the earth-ionosphere waveguide as a detector of a variety of transient geophysical phenomena. A correct interpretation of such results depends critically on understanding the propagation characteristics of the path being monitored. The observed effects will vary depending on time of day, path length, path orientation, magnetic latitude and VLF frequency. This paper provides a brief tutorial of the relevant propagation dependencies for medium to long VLF paths best understood in terms of waveguide mode theory together with results either not previously published, not published in the open scientific literature or whose significance has been little recognised.

**Keywords:** VLF propagation, waveguide mode theory, wave-hop, mode conversion, D region, trans-equatorial propagation

## 1. INTRODUCTION

A move to VLF transmissions at frequencies less than 30 kHz seemed desirable after the First World War, because of their long-range. However the necessary antennas were large, expensive, required high operating power and were competing with a highly level of natural electromagnetic background noise. The available bandwidth was necessarily very small. Following its discovery, short wave radio HF frequencies soon took over long-range communications from LF/VLF.

After the Second World War, interest in VLF was renewed with the establishment of high stability transmitters linked to atomic frequency standards. Phase-tracking VLF receivers could then be used to correct the drift of local oscillators and bring them into line with the overseas frequency standard, once the small diurnal variation in phase was discounted. This application was based on the ability of VLF to deliver a phase coherent signal anywhere in the world. The phase and amplitude of the received signal was typically recorded on charts and later recorded digitally on tape or computers as these new technologies became available. Such records allowed a large number of geophysical and propagation phenomena to be observed and studied for scientific purposes.

The US Navy set up a number of VLF transmitters in the USA and several other countries around the world as a means of maintaining contact with submerged submarines. These phase-stable transmitters used Frequency Shift Keying (FSK). Here the signal switches alternately between two nearby frequencies but always maintains phase coherence after each switch so that phase tracking receivers with a suitable time constant could still lock on to one

CP1286, *Propagation Effects of Very Low Frequency Radio Waves, Proceedings of the 1st International Conference on Science with Very Low Frequency Radio Waves: Theory and Observations,* edited by S. K. Chakrabarti

of the two frequencies. The US Navy subsequently shifted to Minimum Shift Keying (MSK) which allowed the data rate to be doubled still using the same two frequencies but with the possibility of a 180° phase shift when returning to a previous frequency. These signals could no longer be phase tracked. However, putting in a frequency doubler in front of the phase tracking receiver converted the 180° phase jumps back to a coherent phase signal which could then be phase tracked at the doubled frequency. Other more complex techniques have since been developed to track the switching frequencies [1].

Navigation became a new application for VLF propagation with the development of the Omega system from the 1960s [2]. Once again this application was based on the phase stability and low attenuation of the VLF signal over great ranges. The resultant navigation system operated at frequencies between 10.2 and 13.6 kHz and was the first radio navigation system to operate worldwide. A similar VLF navigation system called Alpha was established in Russia and is still in operation. The Omega navigation system was discontinued in 1997 as the satellite-based GPS system took over with much higher positional accuracy and reliability.

This paper provides a tutorial rather than a review of our current understanding of VLF propagation at path lengths and frequencies for which the theory of waveguide mode propagation is relevant. In this theory, waveguide modes are trapped between the surface of the Earth and the base of the ionosphere. Trapping occurs because the VLF electromagnetic wavelength (30km-3 km) is comparable with the 75-90 km height between the base of the ionosphere and the earth. This theory is most appropriate at distances beyond 1000-2000 km as higher order modes attenuate out and the mode structure simplifies. At shorter ranges, many modes need to be summed. In contrast, a wave-hop theory may be more relevant at short distances as fewer hops need to be considered the shorter the path. The wave hop and waveguide mode approaches are thus seen to be complimentary [3] [4].

The study of geophysical disturbances detected at VLF requires some understanding of VLF propagation because the same phenomena may produce quite different results in terms of phase and amplitude deviation depending on the monitored frequency, path length, solar zenith angle and VLF propagation mode. A review of ELF/VLF propagation, mainly as a detector of geophysical phenomena, has been given [5].

The intention in this tutorial is to provide a self-consistent description of VLF waveguide propagation from man-made transmitters based on papers scattered through the literature. Particular attention in this tutorial is given to relevant results that have often been inaccessible to all, rather than attempt a complete review of the many published papers in this field. Figures and data not otherwise referenced are my own.

The classic well-known geophysical phenomena which produce disturbances over a significant part of the earth's surface with durations greater than several minutes are also described. Newer areas of geophysical research are discussed elsewhere in these Proceedings.

## 2. BASIC WAVEGUIDE THEORY

The waveguide theory of VLF propagation was first developed in modern form by Budden

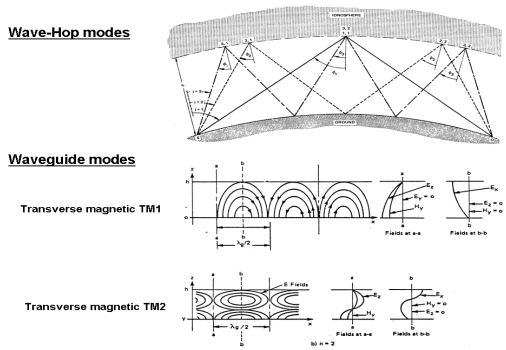


**FIGURE 1**. Wave-hop paths [4] and waveguide-mode electric fields [6].

[7] and subsequently by Wait [8-9] as well as others [10-11]. Calculated values of VLF propagation parameters were given in [12]. These values are still useful in understanding the general dependence of waveguide mode parameters on frequency, reflection height, ionospheric gradient and ground conductivity.

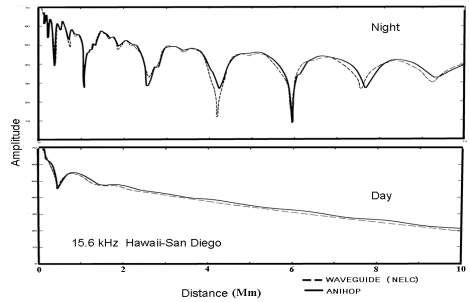


**Figure 2.** Demonstration of the mathematical equivalence of wave-hop and waveguide theory for day and night calculations over a path from Hawaii to San Diego at 15.6 kHz [4].

The equivalence of waveguide and wave hop theory was demonstrated as shown in Fig. 2 [4].

## 2. WAVEGUIDE MODE THEORY

For propagation over a curved earth, the vertical electric field strength between the ground and the ionosphere, assuming a propagation path of uniform height between a vertical transmitter and receiver, can be written as a sum of waveguide modes as

$$E(d) = \frac{k}{(a\sin(d/a))^{1/2}} \sum_{n=1}^{N} G_n \Lambda_n \exp\{-\alpha_n d + j[\varphi_n + \frac{2\pi f d}{c}(1 - \frac{c}{V_n})]\}$$

$d =$ path length

$k =$ transmitter power factor

$c =$ velocity of light

$\Lambda_n =$ nth mode excitation factor magnitude

$a =$ radius of the earth

$\alpha_n =$ nth mode attunuation rate

$\varphi_n =$ nth mode excitation factor phase

$V_n =$ nth mode phase velocity

$f =$ transmitter frequency

The first term in this equation represents the geometric spreading of energy in the waveguide. The summation terms represent attenuating modes each travelling with a slightly different velocity. The coupling between the VLF transmitter and each waveguide mode is given by the excitation factor Λ. The height-gain factor G represents the variation of the electric field with height within the waveguide and is normalised to 1 at the ground.

The first order mode excitation factor for a ground based transmitter and receiver improves as the height of the ionosphere decreases [13]. A decrease in reflection height occurs above a VLF transmitter at sunrise as the effective height of the waveguide decreases from a night-time value of around 90 km to a daytime value of around 75 km. The increase in

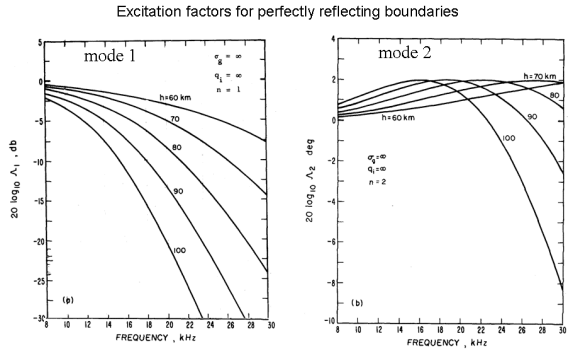


**FIGURE 3.** Excitation factors for the first and second TM waveguide modes as a function of frequency for a range of waveguide heights [13].

first mode field strength at transmitter sunrise on the eastern end of a propagation path can be particularly evident at the higher VLF frequencies where a brief increase in received signal amplitude at sunrise can be produced over long paths as shown in Fig.4 [15] for NPM

(23.4 kHz), NPG (18.6 kHz) and Omega Hawaii (13.6 kHz) as received at Bribie Island near Brisbane.

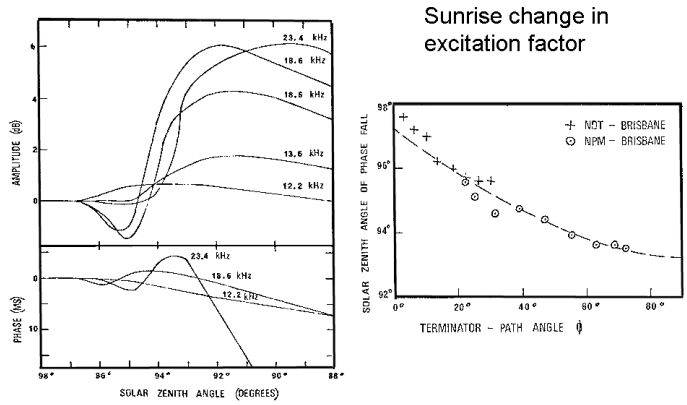


**FIGURE 4.** a **-** Increase in received field strength as the reflection height falls above the transmitter at sunrise with a resultant improvement in first mode excitation factor and related phase changes [15]. b – dependence on path/terminator angle.

In Fig.4, the first effect of sunrise at the higher VLF frequencies for the paths shown occurs around a solar zenith angle $\chi = 97.5^{o}$ as an initial dip in signal strength followed by an increase to a maximum in signal strength at a solar zenith angle which increases with VLF frequency. The first disturbance in phase starts at the same solar zenith angle as the disturbance in amplitude but the point at which the phase starts to move continuously towards the daytime value shifts to higher zenith angles (i.e., earlier times) as the difference in night-day excitation factor decreases. The beginning of sunrise at a 90 km height occurs later than expected because of the shielding effect of the ozone layer at a height of around 30 km. Fig.4 demonstrates that the point of phase turnover is also a function of path/terminator angle and occurs later as the path/terminator angle increases towards $90^{o}$ [15].

The height gain function [13] represents the variation of the vertical electric field of a waveguide mode with height and is normalised to 1 at ground level. At higher VLF frequencies, the curvature of the waveguide causes the field strength to increase with height relative to the flat-earth case and can lead to a whispering gallery or earth-detached mode where much of the energy is trapped near the upper surface of the curved waveguide. Such a mode will be poorly coupled to a ground based transmitter (i.e., reduced excitation factor as seen in Fig. 3). For this reason, excitation of the first mode relative to the second decreases with increasing frequency so that the second mode may be dominant to great distances from the transmitter at the higher VLF frequencies despite its higher attenuation rate.

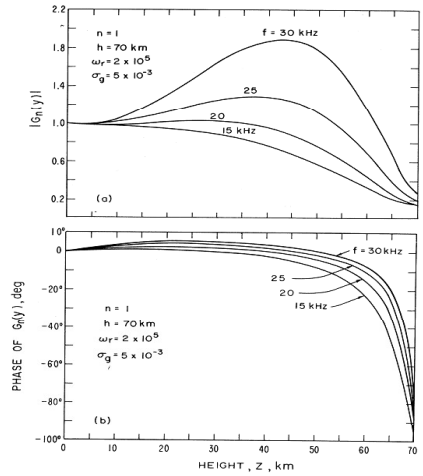


**FIGURE 5.** Height gain factors for the first mode as a function of frequency and height [14].

The modes described thus far are Transverse Magnetic (TM) modes which meet the boundary conditions where the ground can be approximated as an electric conductor (especially over sea water) with a reflection coefficient r = 1 while the ionosphere can be approximated as a magnetic conductor r = -1. With these boundary conditions, as shown in Fig. 1, the TM electric field E at the ionosphere is approximately horizontal. When the propagation path has a component at right angles to the earth's magnetic field, the electrons driven horizontally will attempt to gyrate around the magnetic field line (ExB force).

The ExB force will produce a vertical component of electron motion whose re-radiation will couple to Transverse Electric (TE) modes in the earth-ionosphere wave-guide thus leaking energy from the TM mode into one whose coupling from a vertical ground transmitter would otherwise be negligible. This coupling will vary with geomagnetic dip angle and is maximum for propagation paths at right angles to the horizontal magnetic field lines of the earth at the magnetic equator. The TM to TE coupling will be higher at night due to the higher reflection height of the waveguide and the consequent lower collision rate.

This separation of TM and TE modes seems to have been the expectation in all the studies based on the theoretical methods of Wait. However subsequent full wave studies [11] based on the methodology of Budden revealed a far more complicated situation. Modes of mixed polarization, described as quasi-TM and quasi-TE, were now generated. These modes showed much greater dependence on path magnetic bearing and magnetic latitude. In this paper, the results of Wait, when presented, should be taken as a first approximation.

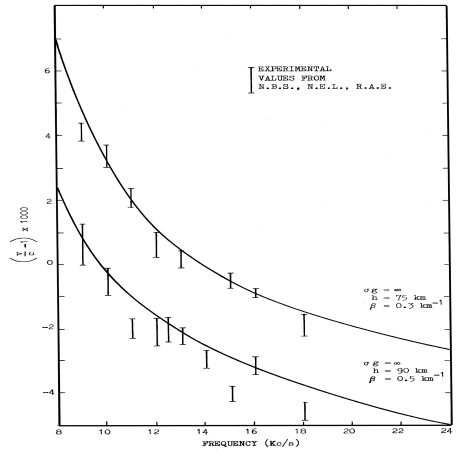


**FIGURE 6.** Observed day and night phase velocities for mode 1 with corresponding theoretical curves of best fit [13].

VLF propagation parameters in daytime are little affected by the earth's magnetic field because of the high collision rate at day-time reflection heights. At night, however, the parameters are increasingly dependent on path azimuth with respect to the earth's magnetic field lines with the strongest effects on paths with an east-to-west propagation component. This dependence becomes extreme at the magnetic equator for westward propagation as discussed in section 5.

### 2.1 modal phase velocity

The cut-off frequency of the TM waveguide modes lies below 10 kHz. As the frequency decreases and the mode cut-off frequency is approached, the phase velocity increases towards infinity and the group velocity decreases towards zero. Man-made transmitters typically operate at frequencies above 10 kHz. The propagation discussed in this paper is for continuous wave transmission where the phase velocity rather than group velocity is relevant. Fig 6 shows observed and theoretically derived values of phase velocity for night and day in the frequency range of man-made transmitters.

Fig 6 shows phase velocity decreasing with increasing waveguide height. As a result, phase velocity is lower at night when the reflection height is around 90 km than in daytime when the reflection height is around 75 km. Consequently a phase-tracking VLF receiver will see a regular diurnal variation in phase with respect to the local phase reference. Early commercial VLF receivers recorded phase in units of microseconds. Now it is preferable for phase to be measured in degrees, phase cycles or centicycles (1/100 of a cycle).

At night, the TM cut-off frequency of the waveguide mode can be seen as the increase in time delay of distant atmospherics propagating at the group velocity. The resultant waveform is called a "tweek" from its distinctive sound. The tweek cut-off frequency at night is reached at around 1.7 kHz where the group time delay is greatest [17][18].

For geophysical purposes, either the phase of the received VLF signal (relative to the phase of a local frequency standard) or the signal strength can be measured. For maximum discrimination it is preferable to record both of these parameters since their inter-relationship reveals much about what changes have occurred in the parameters of the relevant waveguide modes and hence how those changes should be interpreted.

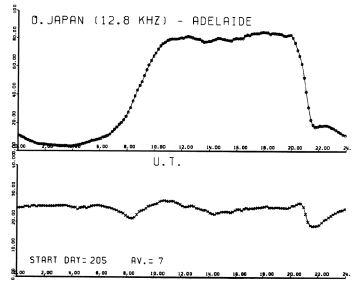


**FIGURE 7.** Typical first mode phase and amplitude diurnal variation observed over a path from Omega Japan to Adelaide at 12.8 kHz.

In early years, diurnal phase variations were typically plotted to match height variation with the phase at night uppermost, as in Fig. 7. In later years, diurnal phase variations were plotted inverted to the above.

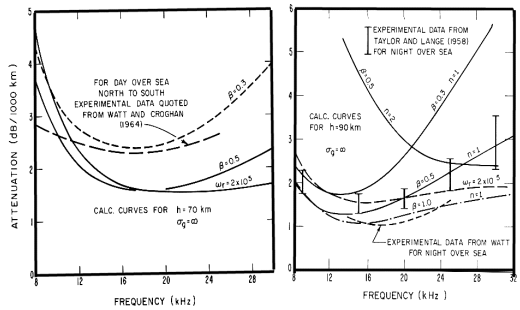


**Figure 8**. Calculated and observed first mode attenuation for day (left) and night (right) with no magnetic field [13].

## 2.2 Modal attenuation rates

Observed and calculated rates of day and night attenuation for the first mode (and night second mode) as a function of frequency are shown in Fig. 8 [13]. Day attenuation of the first mode is in the range 2-4 dB/1000km with 1-2 dB/1000 km at night. The second mode attenuation at night increases rapidly relative to the first mode as the frequency

decreases below about 24 kHz. The calculations shown do not include the effect of the earth's magnetic field which is discussed in the next section.

Attenuation over ground is greater than over sea. The ground conductivity dependence is given in [13]. Evidence for changing VLF attenuation through a sunspot cycle is given in [14] with attenuation falling with decreasing sunset number and its associated hard solar UV ionization.

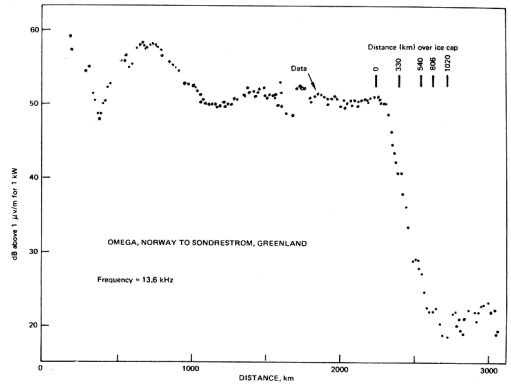


**FIGURE 9.** Omega Norway field strength as a function of distance showing the abrupt increase in attenuation over the Greenland ice cap [19].

The attenuation of VLF signals propagating over deep ice increases considerably as shown in Fig. 9 for a flight from Omega Norway across the Greenland ice-cap [19]. A similar situation applies over Antarctica which throws a shadow on the lea side of the ice-cap for VLF transmitters with propagation paths crossing the ice-cap.

### 2.3. Electron density profiling

Wait early introduced a simple exponential model for the reflecting base of the ionosphere. This model is characterised by two parameters namely an equivalent reflecting height h' and an electron density gradient parameter β. A comparison between such models and an actual D region profile is given in Fig.10a [20]. The exponential model has been used ever since though whether it is always an effective equivalent to actual D region profiles is unclear. Typical use of this exponential profile is in the Long Wavelength Propagation Capability (LWCP) model for calculating VLF signal strength with distance [21]. As well, it is frequently used to characterise D region variations (see section 6).

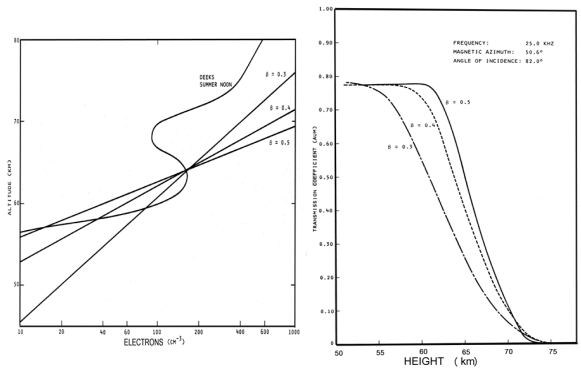


a b

**FIGURE 10.** a- A comparison with a D electron density profile and theoretical exponential profiles with β=0.3, 0.4 and 0.5 [20]; b – calculated penetration of a VLF wave into an exponential ionosphere with the same β values [22].

The reflection of the VLF wave is a continuous process over a range of ionospheric height rather than at a single height. Fig. 10b gives example calculations of wave penetration into the ionosphere for exponential profiles which cover the range normally associated with day-time and night-time ionospheres [22].

Fig.11a shows the seasonal variation of sunrise times at a receiver (Adelaide) and a transmitter (NDT), as a function of solar zenith angle, for a path which is almost north-south. On such a path, the beginning of path-sunrise will swap between the transmitter and receiver depending on time of year. There will also be two times during a year when the path will be parallel either to the sunrise or sunset terminator, as shown in Fig.11a.

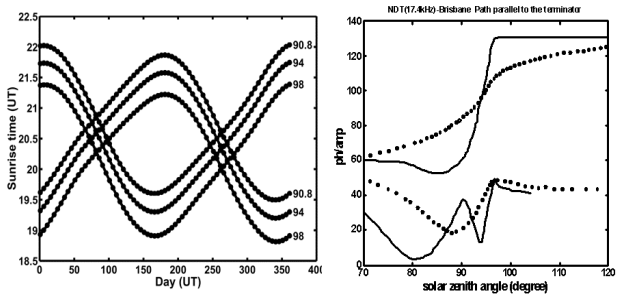


a b

**FIGURE 11** a –Seasonal variation of sunrise times over a year for the path NDT to Adelaide at three different solar zenith angles; b-variation of phase and amplitude at sunrise and sunset for a VLF path (NDT – Bribie) when parallel to the sunrise and sunset terminator.

Fig. 11b compares the variation of observed phase and amplitude over the path NDT, Japan, to Brisbane at times when the path is parallel to the sunrise and sunset terminator. There is a great asymmetry between the fall in height at sunrise and the much slower rise at sunset as seen in the changing phase patterns. The reason for this discrepancy is found in the contest between sources of ionization and recombination. Relevant electron density profiles during the night and at sunrise are shown in Fig. 12a and b.

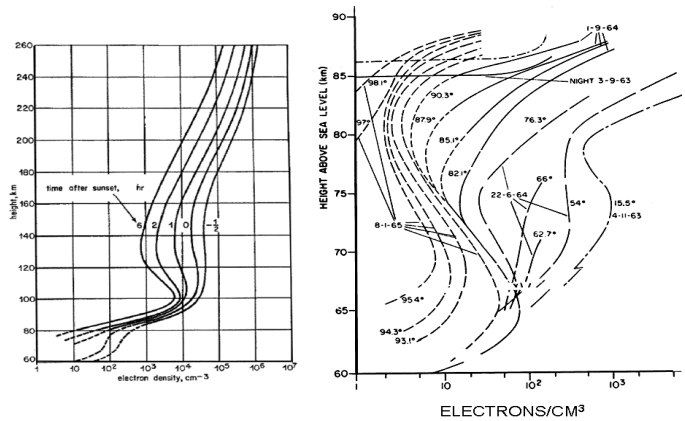


a b

**FIGURE 12.** a –Night electron density profiles from the base of the ionosphere where VLF waves reflect up to the main F2: b – Sunrise changes in electron density profiles with solar zenith angle showing the development of the C layer followed by the development of the subsuming D layer.

Fig. 12a plots electron density profiles as a function of time after sunset and shows the relationship between the bottom of the ionosphere at night where VLF radio waves reflect, and the main part of the F2 responsible for HF reflection [23].

Fig. 12 b plots variations in electron density through sunrise and beyond as a function of solar zenith angle and as observed at a mid-latitude site [24]. The C layer forms first from the detachment of electrons from negative ions built up by cosmic ray ionization during the night. This, along with the abrupt increase in solar ionizing radiation, explains the steepness of the sunrise phase change in comparison with sunset. The latter responds only to the decrease in UV and subsequent slow decay with electron recombination. Following the formation of the C layer, the D layer builds with solar ionization filling in the electron profile trough.

## 2.4 Middle latitude magnetic field effects

The non-reciprocity of field-strength for VLF wave propagation across the Earth's magnetic

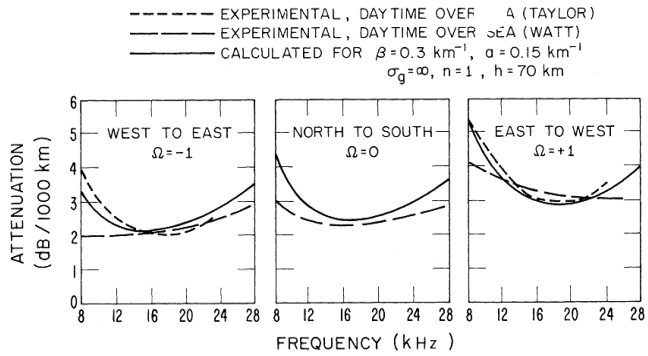


**FIGURE 13.** The modelled variation of first mode attenuation with magnetic bearing [13].

field was established experimentally by Crombie [25]. The dependence of both attenuation and phase velocity on the direction of propagation across the Earth's magnetic field was theoretically derived from the developing wave-guide mode theory of VLF propagation [13].

Subsequent developments with full wave modelling revealed a more complex process [26]. In all theoretical studies, VLF attenuation was found to be greater for propagation to the west than for propagation to the east. This difference increases with decreasing magnetic dip angle and as the angle between the path and the magnetic meridian becomes orthogonal. The magnetic field dependence, as for other VLF propagation parameters, is least in daytime. Extreme effects occur at the magnetic equator at night as discussed in section 5.

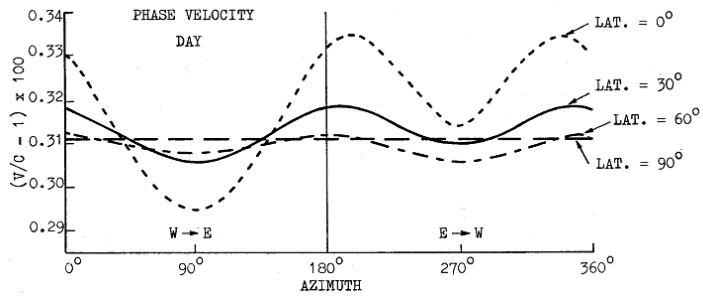


**FIGURE 14.** First mode phase velocity in daytime as a function of magnetic bearing and latitude [27].

Full wave calculations for the day-time variations of VLF first mode phase velocity with magnetic azimuth at various latitudes are shown in Fig. 14 [27] as calculated at 10.2 kHz. The corresponding night values are shown in Fig.15 [27]. The dependence of phase velocity on the direction of propagation relative to the earth's magnetic field as shown in Fig.14 is small at all latitudes. In contrast, the phase velocity at night shows a trivial

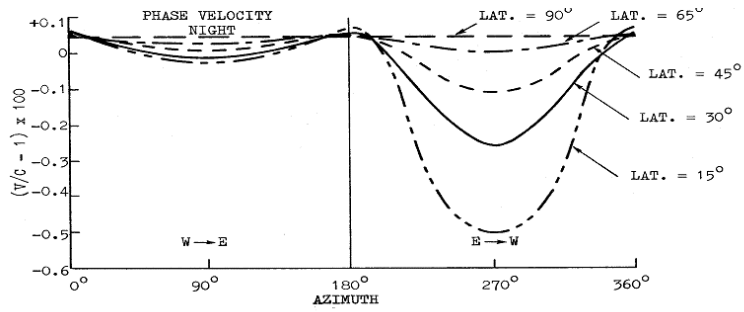


**FIGURE 15.** First mode phase velocity at night as a function of magnetic bearing and latitude at 10.2 kHz [27].

variation with path azimuth for west to east propagation but propagation from east to west shows a very strong dependence on magnetic latitude increasing in magnitude as the equator is approached. Note that values below $10^0$ latitude are not shown for the very good reason that the authors were unsure of their results as the modal structure then became extremely complex. This point and this diagram are examined again in section 5.3.

**Table 1**. Non-reciprocity of middle latitude diurnal phase shifts

| Path | Length km | Freq. kHz | Date | days | ΔΦ (W->E) cec | ΔΦ (E->W) cec | Diff % |
|---|---|---|---|---|---|---|---|
| Haw-Jap | 7150 | 13.6 | Sep. 1982 | 20 | 80.8 ± 4 | 101.6 ± 4 | 26 ± 4 |
| | | 11.3 | Sep. 1982 | 20 | 79.4 ± 2 | 96.6 ± 3 | 26 ± 4 |
| | | 11.3 | Aug. 1977 | 23 | 83.7 ± 4 | 104.4 ± 6 | 25 ± 4 |
| | | 10.2 | Sep. 1982 | 20 | 83.7 ± 2 | 100.8 ± 4 | 21 ± 4 |
| Haw-N.Dk | 5990 | 11.3 | Aug. 1977 | 23 | 72.0 ± 2 | 78.5 ± 2 | 9 ± 2 |

Fig. 15 shows that the phase velocity of the first mode at night decreases for propagation to the west with respect to propagation to the east. Combined with a daytime phase velocity variation which is much less, the result is that the diurnal phase shift between day and night is higher for westward than for eastward propagation. The difference increases as the magnetic equator is approached. This east-west asymmetry is well known and was easily seen in the Omega system. Non-reciprocity in diurnal phase variation ΔΦ measured between Omega Japan and Omega Hawaii, Omega Hawaii and Omega North Dakota is shown in Table 1. Here the diurnal phase shift from Hawaii to Japan is some 25% higher than

from Japan to Hawaii. The diurnal phase shift from North Dakota to Hawaii is only some 9% higher than for the west to east direction because of the higher average magnetic latitude of this path.

It is tempting to conclude from Fig.15 that the Omega results there shown could be extrapolated to an even higher east-west asymmetry in diurnal shift at the magnetic equator. On the contrary paths, paths from Omega transmitters (10.2-13.6 kHz) propagating westward across the magnetic equator showed a strong reduction in diurnal phase shift and reduced signal strength at night. The received phase and amplitude of the signal was erratic compared to middle latitude paths of similar length. Phase cycle slipping (section 4) during the morning sunrise transition was common on such westward propagating trans-equatorial paths. In recognition of this fact, the Omega navigation system defined deselection zones for each transmitter where such westward trans-equatorial signals were not to be used for navigation at night. These zones were euphemistically referred to as areas of "modal interference".

The biggest Omega system failure resulted from the construction of the Omega transmitter in Liberia which was meant to cover the Atlantic. This transmitter was almost on the magnetic equator and the signal proved useless for navigation for westward trans-equatorial propagation at night. The propagation asymmetries which occur on trans-equatorial paths are examined in greater detail in section 5.

## 3. DIRECT MODAL INTERFERENCE

A ground-based VLF transmitter excites all the possible TM modes in the waveguide. The attenuation increases with mode order so that the summed signal simplifies with distance

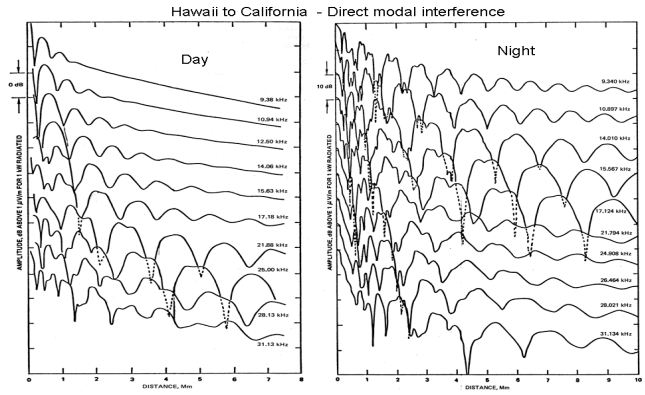


**FIGURE 16.** Computed VLF signal strength for day and night over a fixed path showing the variation of mode interference with frequency and distance for day and night conditions [28].

as the higher modes die out. Theoretically calculated signal strength as a function of distance and frequency from a VLF transmitter are shown for day and night in Fig.16 [28]. These calculations are not necessarily accurate for specific paths but show the general variation of direct modal interference expected for propagation over a mid-latitude path between Hawaii and California.

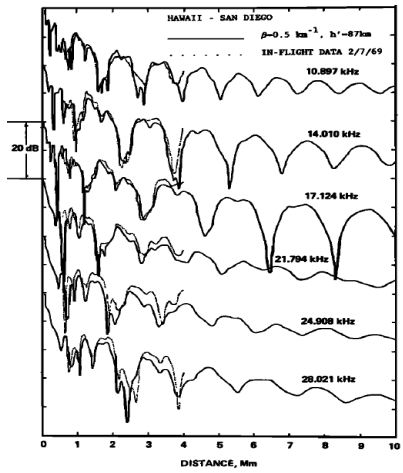


**Figure 17.** Comparison between aircraft measurements of VLF signal strength with distance at a number of frequencies and calculated signal strength [29].

As shown in Fig. 16, the modal interference pattern is quite complex in the vicinity of the transmitter, particularly so at night. At greater distances, the modal interference pattern simplifies with distance to what is essentially a two mode fading pattern. The deepest fades occur at distances and frequencies where the two modes become almost equal. At higher frequencies than this, the second mode can now be the dominant mode and the oscillations are produced by interference from the weaker first mode and higher order modes.

A large number of radial flights from VLF transmitters were carried out by the USA to test the ability of theoretical waveguide models to match observed signal strength patterns as a function of distance and frequency for both day and night. Fig. 17 shows such a comparison for flights from Hawaii to San Diego [29]. Because of the Cold War, flights concentrated on the Northern Hemisphere where communication with submarines could be critical.

In 1980, five RAAF flights were made from Adelaide, Australia, in daytime, refuelling near the NWC VLF transmitter. These flights were made in order to test the relative performance of hybrid Omega navigation receivers in the Indian Ocean where pure Omega navigation receivers proved inadequate. These day-time flights serendipitously mapped out the location of the first two major signal minima in the propagation field of

NWC with results shown in Fig. 18a [30]. The consistency of these locations over several flights was followed up by plotting the location of such daytime minima as a function of frequency from the more numerous US flight data. The remarkably consistent day-time results thus obtained are shown in Fig. 18b [30].

One of the few westward trans-equatorial flights at night was made by the US Navy between Hawaii and Samoa. This produced unusual results which were theoretically investigated and found to result from large deviations from normal modal behaviour in the vicinity of the magnetic equator [31]. This matter is discussed further in section 5.

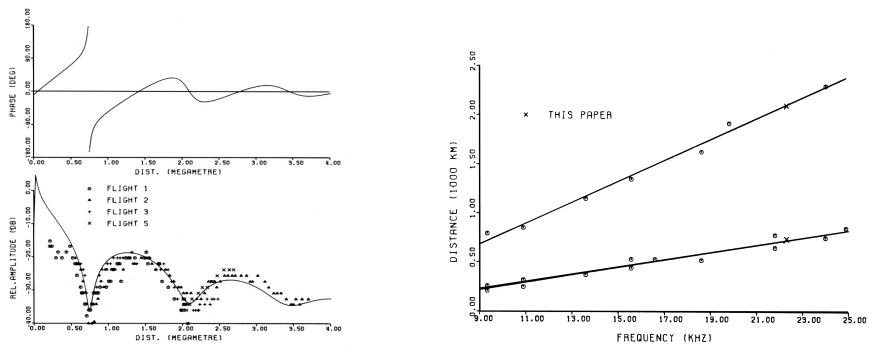


a b

**FIGURE 18.** a - Aircraft measurement of NWC signal strength with distance in day-time at 22.3 kHz [30]: b - location of the first two major nulls in the day-time modal interference pattern as a function of frequency deduced from U.S. aircraft flights [30].

Because of their high variability in both phase and amplitude, observations over such trans-equatorial paths are more reliably made at fixed receiver sites where the diurnal patterns can be averaged over many days (e.g. [32]).

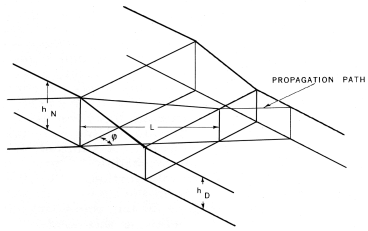


**FIGURE 19.** A simple model of the fall in VLF reflection height at sunrise and the length of the height change L for a VLF path crossing the terminator at an angle Φ.

# 4. TERMINATOR-GENERATED MODAL INTERFERENCE

The existence of wave-guide mode conversion at the height discontinuity at the wedge-shaped change in waveguide height occurring at the sunrise and sunset terminator

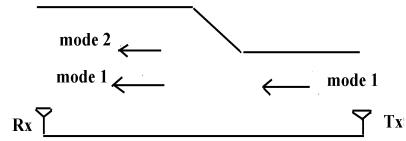


**FIGURE 20.** Propagation through a height transition for a transmitter in daylight and a receiver in darkness showing mode conversion.

(Fig.19) was first recognized experimentally by Crombie [33] and verified by Walker [34], with subsequent theoretical derivation by Wait [35]. The process involved is best understood by taking a waveguide model with an abrupt step in height between day and night. For the electromagnetic profile of the electric field to remain continuous, multiple modes have to be summed in order to match fields across the step (analogous to a Fourier expansion). Mode conversion at a more realistic wedge-shaped height transition (Fig.19) was achieved by breaking it into a series of height steps, each of which had a step model applied. A more sophisticated method was developed in [36].

Fig. 20 shows an example of a VLF transmitter at the eastern end of a propagation path during a sunrise transition as the height discontinuity moves towards the receiver. In the simplest case, as investigated by Crombie [33], all but the first mode dies out in the day section of the path as the day path lengthens. This first mode generates a significant amount of second mode at the sunrise discontinuity (as well as some higher order modes) in order to match fields across the discontinuity. There is thus an interference pattern in the night path between the first and second modes. This interference pattern is fixed with respect to the height discontinuity and is driven down the path as the night path component diminishes. The resultant oscillations in field-strength and phase at the receiver yield valuable information about the relative mode-conversion amplitudes, phase velocities and attenuation rates of the night propagation modes.

If the same waveguide model shown in Fig. 20 has the transmitter and receiver transposed (i.e. the sunrise is first at the receiver and last at the transmitter) then an entirely different situation apparently applies as is shown in Fig. 21.

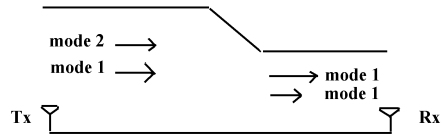


**FIGURE 21.** Propagation through a height transition for a transmitter in darkness and a receiver in daylight showing mode conversion.

Here the transmitter is in darkness and the greater waveguide height allows a significant component of mode 2 to be generated producing a modal interference pattern in the night path. At the sunrise terminator, part of mode 2 is converted to mode 1 with the remaining direct component of mode 2 dying out very rapidly in the day path because of its higher attenuation. The phase of the additional mode 1 component follows the phase variation of mode 2 in the night path and thus causes the summed mode 1 in the day path to oscillate in phase and amplitude in step with the night interference pattern.

Although the two cases of Figs. 20 and 21 appear to be completely different, reciprocity says that the results will be exactly the same, if magnetic field effects are ignored. In both cases, the modal interference fading observed at the receiver is determined by the relative phase velocity of modes in the night path. The presence of the earth's magnetic field produces the non-reciprocity actually observed and discussed previously and in the following section.

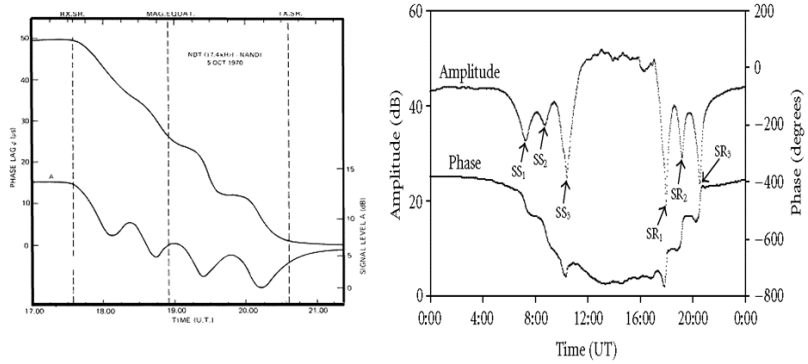


(a) (b)

**FIGURE 22.** a - Phase and amplitude variations produced by mode conversion as the sunrise terminator traversed a path between NDT (17.4 kHz), Japan, and Fiji; b – Diurnal phase and amplitude variation for NWC (19.8 kHz), Western Australia, received in Fiji.

An example of the sunrise transition over a path from NDT Japan (17.4 kHz) to Fiji [37] is shown in Fig.22a. This is a path length and frequency which produces a simple two mode fading sunrise transition pattern with fades and phase oscillations increasing in depth as the night path shortens. Fig22b shows an example of a complete diurnal pattern of NWC, Western Australia (19.8 kHz) received in Fiji [38]. A vast literature of such examples exists going back to the 1960s (e.g.[33] [39]). Weaker mode conversion at the more extended sunset transition produces reduced fading in comparison with the much stronger fading in signal strength and phase oscillation during the sunrise transition. The abrupt reversals in phase at the completion of the sunset transition in Fig.19b and at sunrise indicates that, at this path length and frequency, direct modal interference from the transmitter is still present producing a reduction in diurnal phase shift when the whole path is in darkness.

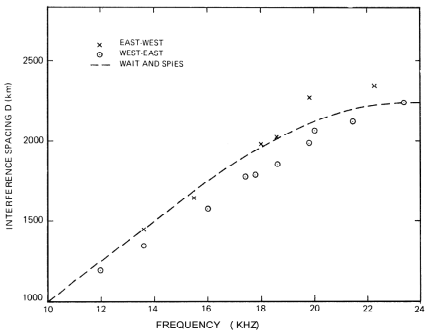


**FIGURE 23.** Measured values of the sunrise modal interference spacing *D* as a function of frequency for both east to west and west to east VLF propagation.

The distance *D* moved by the terminator along the propagation path between signal minima is a measure of the difference in phase velocity between the first and second modes [33] and is given by the simple relationship

$$D = \frac{\lambda_1 \lambda_2}{\lambda_2 - \lambda_1}$$

where $\lambda_1$ and $\lambda_2$ are the phase velocity wavelengths of the first and second mode.

Values of *D* as a function of frequency have been made by many people with a considerable amount of agreement (e.g. [40][41]). An example (Fig.23) provides evidence of higher values of *D* for propagation to the east relative to propagation to the west at middle latitudes [41]. Values of *D* decrease with decreasing frequency as shown.

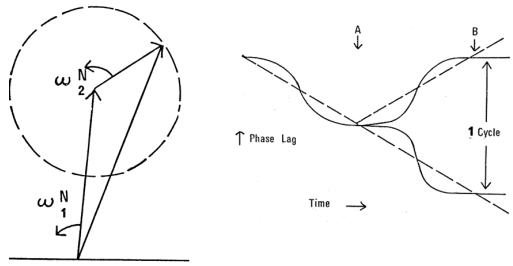


(a) (b)

**FIGURE 24.** a – summation of two modes of different phase velocity and the phase and amplitude oscillations thus produced: b – the appearance of phase cycle slipping when the dominant modes swap over relative amplitudes with time.

The choice of the solar zenith angle as the appropriate reference point in the terminator height discontinuity proves to be critical to the accuracy of the D measurement, as pointed out in [42]. This becomes relevant because the angle between the terminator and the propagation path will vary along the propagation path and if the choice of reference solar zenith angle is incorrect then so will be the measurement of D [41] [43].

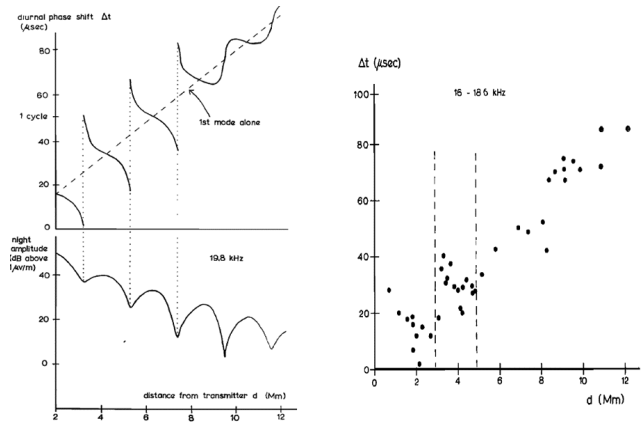


(a) (b)

**FIGURE 25.** a - Calculated variation of diurnal phase shift as a function of distance when the second mode is more strongly excited at night than the first mode [44]: b - Corresponding experimental observations in the frequency range 16 – 18.6 kHz [44].

Phase cycle slipping occurs when dominance between two propagating modes is swapped either as a function of distance or as a function of time. This is best understood by considering Fig. 24a. Here a mode vector of lesser amplitude rotates with respect to the dominant mode because of their differing phase velocities. The resultant interference produces an oscillation in phase and amplitude about that of the dominant mode, as seen during the sunrise transition in Fig.22 and with distance and signal strength in Fig.16. If the smaller mode vector should grow with respect to the previously dominant mode, then the total vector will swing around the base of the first vector and a cycle of phase will be added to the phase pattern as in Fig.24b.

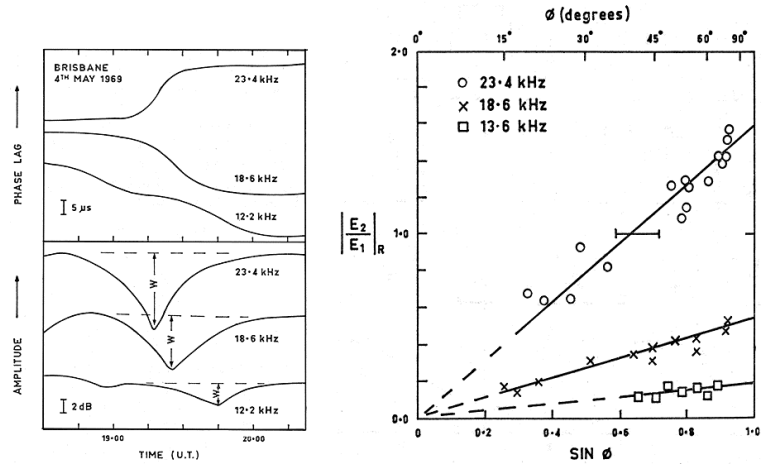


**FIGURE 26** a – Phase and amplitude oscillations for the last signal minimum before path sunrise at several frequencies b – The ratio of the second to first mode components as a function of solar zenith angle [16].

For direct transmitter- generated modal interference, the second mode at night will be the dominant mode with the first mode causing the oscillation in phase and signal strength. At some distance however, the second mode because of its higher attenuation will fall in amplitude below that of the first mode which will then be the dominant mode at all greater distances. The resultant effect on diurnal phase shift as a function of distance is as shown in Fig.25a as theoretically calculated in [44]) and as observed in Fig.25b [44]. Note that when the second mode is dominant, the diurnal phase shift decreases with distance before undergoing an abrupt cycle jump at each signal fade.

For mode conversion during the sunrise transition, the night path steadily decreases and the received second mode grows in amplitude relative to the first until it may exceed it. When this happens, phase cycle slips will occur at all subsequent fades. Observed examples of this dependence on frequency are shown in Fig.26a for the last fade of sunrise path transitions as observed over a path from Hawaii to Brisbane at frequencies ranging from 12.2 to 23.4 kHz [16]. As the frequency increases, the last fade of the sunrise transition deepens as the second mode becomes stronger until it exceeds that of the first mode for the last fade at 23.4 kHz, resulting in a phase cycle slip. Note also that the distance of the last fade from the receiver increases with increasing frequency because the difference in phase velocities of the first and

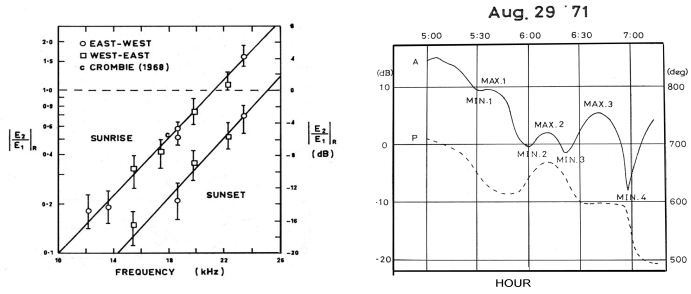


a b

**FIGURE 27.** a – Ratio of the second to the first mode at the last signal minimum of path sunrise and the first signal minimum of sunset as a function of VLF frequency. b – Sunrise phase and amplitude variation over the path NWC (22.3 kHz) received in Inubo, Japan [45].

second modes become less and their interference spacing D becomes greater. The last fade occurs when the midpoint of the terminator height transition (approximately $\chi = 93.5^{o}$) is at a distance of D/2 from the receiver.

Fig.19 shows that the distance L of the propagation path through the height transition at the terminator will vary with path-terminator angle φ. Mode conversion weakens as the angle between the past and the terminator decreases, as is shown in Fig.26b [41]. Fig.26b plots the ratio of the second mode to the first mode at the last signal fade of the sunrise transition as observed at a range of frequencies on paths which have the same bearing to Brisbane. This ratio is found to be a linear function of sin φ.

Fig. 27a shows how the ratio of the second and first modes measured at the last signal fade of path sunrise and the corresponding first signal fade of sunset varies with frequency when the terminator-path angle is high and mode conversion at its maximum [41]. In Fig. 27a, the first mode is always dominant below a frequency of some 21 kHz so that phase cycle slipping on mid-latitude paths can not occur below this frequency on paths which meet the Crombie-model criteria. Above this frequency, the second order mode during the last signal fade and possibly at previous signal fades will dominate producing phase cycle slips unless the path-terminator angle is such that this ratio is diminished below 1, as shown for the 23.4 kHz path (Hawaii-Brisbane) of Fig. 26b.

For the sake of clarity, the discussion so far has been limited to paths in which only the first mode in daytime and the first and second modes at night are relevant. Other path

lengths and frequencies may require a greater combination of modes to explain but constitute a simple extension to the above by adding more rotating vectors. An example of such a situation has been explored in [45] for a path of 6950 km between NWC and Inubo at 22.3 kHz. The observed uneven modal interference spacing and the distorted phase pattern during the sunrise transition was found to result from both the first and second modes being significant at the receiver in day-time. Similar results over short paths were found in [46]. Unpublished results of NWC received at various distances in Australia show a rapid variation in phase and amplitude and diurnal phase shift due to the presence of additional modal components.

# 5. TRANSEQUATORIAL MAGNETIC FIELD EFFECTS

The greatest controversy in VLF propagation theory and experiment has been over the unusual characteristics of westward propagating trans-equatorial VLF signals. This section examines what is known experimentally and theoretically.

### 5.1 VLF band 18.6-24 kHz - observation

The original recognition of the unusual propagation characteristics of VLF trans-equatorial paths propagating east to west were made based on reception of NPG/NLK, Seattle as received in Adelaide [47]. Fig. 28 shows the form of the diurnal phase and amplitude over this path along with similar results for similar transmissions received in New Zealand [48]. The characteristics, which were anomalous at the time, are best understood by comparing the sunrise variations in Fig.28 with those of the west to east trans-equatorial propagation path from NDT at 17.4 kHz received in Fiji (Fig. 22a). The last two signal fades in the sunrise transition of NPG/NLK are as expected but the occasional cycle slip associated with the deep third last fade was completely out of step with the Crombie picture, particularly with the long single mode day path at this time. The relationship of this anomaly with the magnetic equator was established [50] by examining the diurnal phase and amplitude variations of the NLK/NPG signal at a range of distances to a number of locations in Australia. The possibility of long path round-the-world interference as a cause of the observed anomalies was examined and ruled out experimentally [47].

Similar results for NPG (18.6 and 24 kHz) and WWVL (20 kHz) received in New Zealand prior to the recognition of their relationship with the magnetic equator were given in [48] and are also shown in Fig.28. The magnetic equator relationship for the New Zealand results was subsequently confirmed in [49] and the absence of such variations over west to east paths pointed out as indicating a basic non-reciprocity for trans-equatorial paths which could only be due to a magneto-ionic effect of the earth's magnetic field on VLF reflection at the ionosphere. Subsequent observations over very much shorter paths confirmed this result.

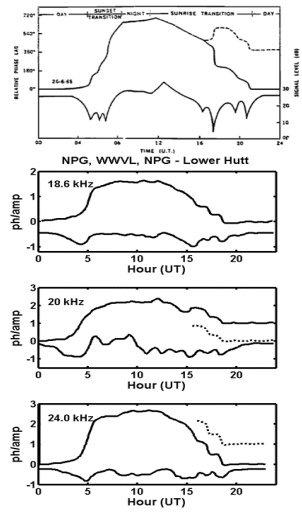


**Figure 28.** West to East trans-equatorial diurnal phase and amplitude variation of NPG (18.6 kHz) received in Brisbane (top) along with NPG (18.6 kHz, and 24.0 kHz) and WWVL (20 kHz) received in Lower Hutt, New Zealand [48]. The occurrence of cycle slipping on these paths is also indicated

It is worth remembering that at this time there were no VLF transmitters in the southern hemisphere so that such trans-equatorial results could not be verified by receivers in the northern hemisphere. Such results did not meet the then current theoretical expectations. A detailed examination of the diurnal phase shift and terminator phase and amplitudes variations over the NPG/NLK-Brisbane path was made [51] which indicated that the magnitude of diurnal phase shift over the path from NLK/NPG to Bribie Island was consistent with non-equatorial measurements and the anomalous modal interference spacing was a result of a decrease in phase velocity of the second mode in the equatorial section of the path.

The theoretical resolution of these results [52], as discussed in section 5.3, was not published in the open scientific literature at the time and thus remains little known even today.

### 5.2 VLF band 10-14 kHz – observations

The Japanese and Hawaiian Omega navigation transmitters provided an excellent range of trans-equatorial propagating paths to Australia many of which were east to west.. Publication of these extensive results is currently being prepared for publication. A sample of trans-equatorial Omega diurnals received over east to west paths is shown in Fig.29 for paths from Omega Argentina to McPherson, Kansas [53], Omega Hawaii to Brisbane and Melbourne, and Omega Japan to Cocos Island. A similar result was reported by Kikuchi [54].

More recent results have been given for Omega Hawaii received in New Zealand [32 ] and Omega Reunion received in Italy [55]. In all these cases, the anomalous effect consists of a reduced diurnal phase shift and a brief reversal in the direction of phase movement during the sunrise and sunset transitions, a quite different and much simpler pattern to that seen at 18.6 kHz and higher VLF frequencies. The anomalous phase pattern was first published in the open literature for Omega Hawaii received near Brisbane [56]. See also examples in [57] some of which are included in Fig. 29.

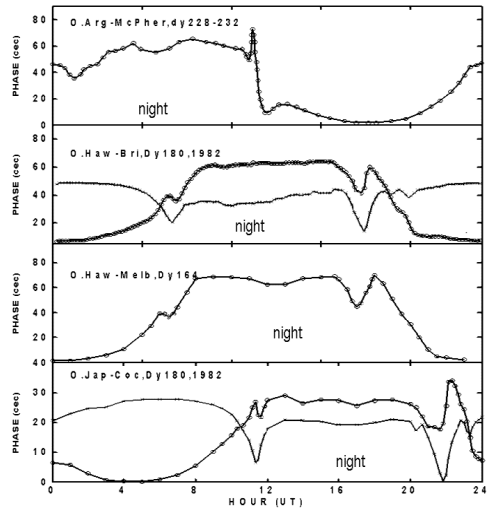


**Figure 29.** Diurnal phase and amplitude variations for Omega Argentina, Omega Hawaii and Omega Japan received over a variety of East to West trans-equatorial paths.

### 5.3 Theory of westward trans-equatorial VLF propagation

The first theoretical report published in the scientific literature showing significant changes in modal characteristics in the vicinity of the magnetic equator for westward trans-equatorial propagation seems to be that made by Bickel [58] for a path from NPM Hawaii at 23.4 kHz received in Samoa. The first successful work to theoretically reproduce experimental observations in any detail as a function of trans-equatorial path length was made by Snyder in his Ph.D. thesis and published as an internal report [59]. This work used the experimental observations of Lynn [50] for NLK/NPG received in Australia as the basis for comparison between observation and theory. The successful theoretical result for the variation of received sunrise modal interference pattern with trans-equatorial path distance is shown in Fig.30. Fig.30 shows the successive expansion of the modal interference spacing across the magnetic equator followed by successive decreases as a new normal fade appears beyond the equatorial zone as the receiver distance increases.

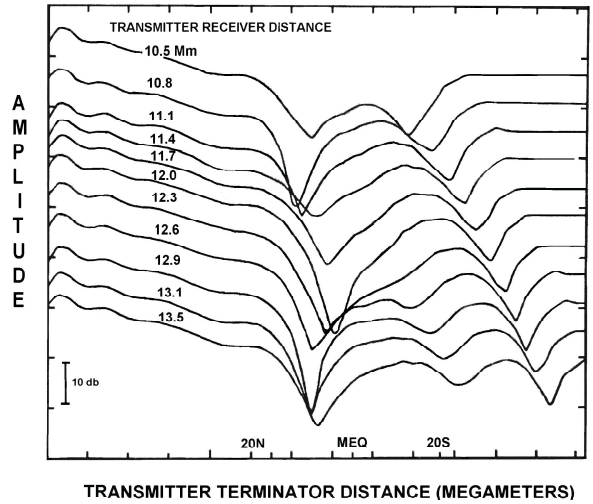


**Figure 30.** Computed signal strength of NPG (18.6 kHz) as a function of receiver distance over trans-equatorial paths to Australia [59] for comparison with observation [50].

The work of Snyder [59] was known to very few and has remained so ever since. Baba in ignorance of these prior results independently calculated the theoretical variation in mode structure for the path NPG/NLK to Adelaide [60]. In so doing he provided a valuable service in verifying the calculations of Snyder though in a Japanese journal once again not widely read by VLF workers. A comparison between the mode structure deduced by Snyder and that of Baba is shown in Fig.31 where the excellent agreement between these independent theoretical calculations of modal phase velocity and attenuation for the path NLK to Adelaide at 18.6 kHz is evident.

The reason these results were not obtained by Wait in his earlier theoretical studies lay in inadequate allowance for the coupling of modes at the ionosphere caused by the earth's magnetic field. This can produce quasi-TM and quasi-TE modes with unusual polarizations, particularly at the magnetic equator. This coupling can destroy the simple separation of modes into TM and TE and cause problems in mode numbering. References to experimental observations in this paper labelled as due to mode 1 and mode 2 are to the apparent dominant modes. A theoretical study may well label them differently when both quasi-TM and quasi-TE modes are considered.

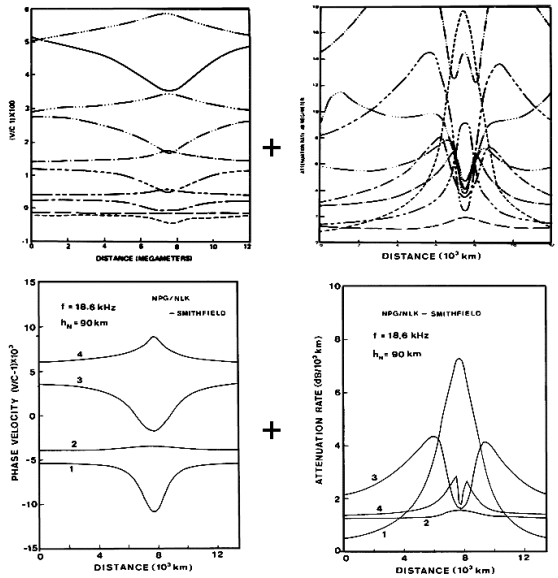


**Figure 31**. Computed phase velocity and attenuation for westward propagating modes, over the path NPG to Adelaide, made by Snyder [59] and Baba [60] demonstrating agreement over the major changes occurring in the vicinity of the magnetic equator.

Detailed theoretical calculation of modal property changes for east to west propagation at Omega frequencies, particularly near the magnetic equator, were made in a report by Morris and Gupta, 1983, under contract to the then US Naval Electronics Laboratory (private communication) but apparently never published in the open literature. These results are shown in Fig. 32 as a function of magnetic latitude and geomagnetic bearing. As expected, the phase velocity of the night mode shows almost no variation with latitude for west to east propagation but decreases rapidly with decreasing latitude for east to west propagation (as also seen in Fig.15). This result produces the well-known increase in diurnal phase shift over east to west middle latitude paths in comparison with west to east diurnal phase shifts. However at magnetic latitudes below 10° a point of modal degeneracy occurs at which energy is transferred from the normal propagating mode to a temporary mode with a very high phase velocity before re-coupling at the other side of the magnetic equator.

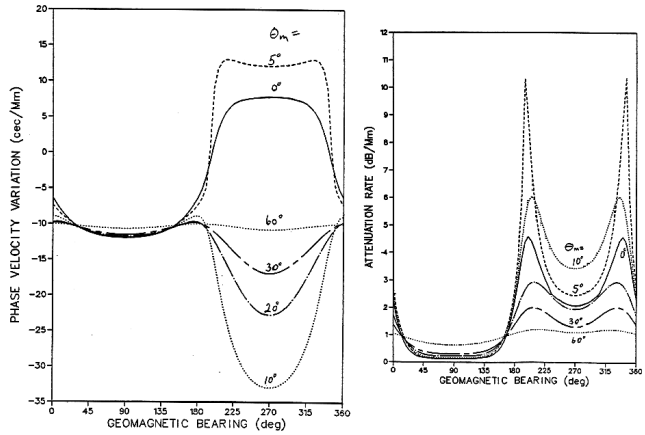


**Figure 32.** Phase velocity and attenuation at 13.6 kHz as a function of magnetic latitude and bearing showing abrupt modal velocity and attenuation change in the vicinity of the magnetic equator for westward propagation (Morris and Gupta, 1983).

As will be subsequently shown, Morris and Gupta had in fact solved the problem of the anomalous Omega diurnal propagation shifts described above. However this does not appear to have been pursued. Instead the US Coast Guard Omega Project Detail used such results to prepare exclusion maps which showed large areas for westward trans-equatorial propagation from all Omega transmitters in which such transmitters were not to be used for navigation at night because of their signal instability, unpredictable diurnal phase shifts and reduced signal strength.

Once again, the problem of night-time westward trans-equatorial propagation frequencies was independently solved, this time at 14.9 kHz by Russian mathematicians Perel and Stesik in 1997 [61]. Once again the import of these results was not recognised. These results confirmed the effect of degeneracy in shifting energy into a temporary trans-equatorial mode as can be seen in Fig.33. A recent theoretical paper [62] supports the concept that modal degeneracy can result in a transfer of modal energy.

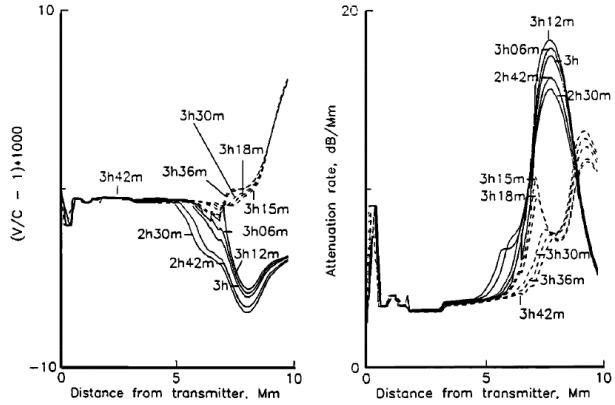


**Figure 33.** Calculated phase velocity and attenuation as a function of time and distance for a westward transequatorial path at 14.9 kHz [61].

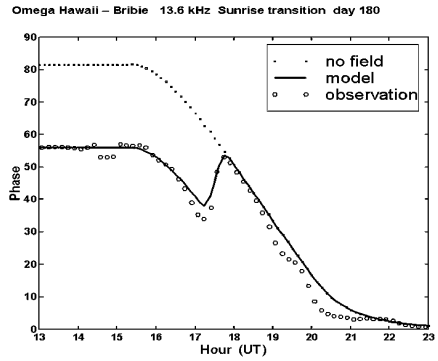


**Figure 34.** Observed sunrise phase pattern over the path Omega Hawaii to Bribie, Australia, and the corresponding simple model involving a short distance of high VLF phase velocity in the vicinity of the magnetic equator.

Fig. 34 shows how a simple model containing a short distance at the magnetic equator where the phase velocity is very high at night can explain both the observed reduction in diurnal phase shift, the phase reversal during the sunrise transition and its location. The path shown is for Omega Hawaii received near Brisbane at 13.6 kHz. The reduced diurnal phase shift results from the night-time propagation path now having a higher average phase velocity which reverts to a non-equatorial night phase velocity as the terminator moves westward

beyond the equatorial region now in daylight. Such an explanation was also suggested by Kikuchi [54].

The same pattern is seen during the sunset transition with the phase reversal being less in magnitude as it is spread over a longer time interval because the day-night height transition distance is much longer at sunset than at sunrise (as shown in Fig.11b).

Finally it must be emphasised that no anomalous modal changes occur at night for eastward propagation across the magnetic equator. The paper by Chilton and Diede [63] is sometimes referenced as the first example of a trans-equatorial anomaly in comparing diurnal phase shifts over paths from NBA, Panama received over a trans-equatorial eastward path to Tucaman, Brazil and over a non-equatorial path of similar length to Boulder, USA. As is discussed in [64], the difference between these two paths is indeed due to the earth's magnetic field which only acts significantly on the westward non-equatorial NBA- Boulder path in comparison with the eastward trans-equatorial path. The latter does not differ from middle latitude values of diurnal phase shift when modal interference is taken into account.

# 6. Geophysical disturbance

The classic geophysical disturbances observed at VLF are Polar Cap Absorption (PCA), Sudden Phase Anomaly (SPA), also referred to as a Sudden Ionospheric Disturbance (SID) and solar eclipses. Their main characteristics are briefly set out below.

## 6.1 Polar Cap Absorption (PCA/SPE)

VLF propagation paths which traversed auroral zones were found to be very sensitive to particle precipitation as measured both by the absorption of HF signals and from riometers operating at high latitudes. In particular, solar protons were found to penetrate deep into the atmosphere producing ionization below the normal height of the ionosphere. The resultant decrease in VLF reflection height was greatest at night thus producing a reduction in diurnal phase shift [65]. The term PCA has become an obsolete term at VLF having been replaced by the more accurate term Solar Proton Event (SPE). Coronal mass ejections from the sun are the most common source of such proton events which may last for more than one day and are also associated with large-scale changes in the magnetosphere as evidenced by abrupt changes in the DST (reduction) and Ap (increase) indices. These typical relationships are shown in Fig. 35 as seen over high latitude VLF paths.

A recent examination of the SPE can be found in [66]. Electron precipitation also occurs in the auroral zone (producing aurora!) and will affect VLF paths but their characteristics are far more variable.

## 6.2 Sudden Ionospheric Disturbance (SPA/SID)

Solar flares which have strong hard UV and X-ray component have long been known to increase ionization in the D region resulting in a further increase in VLF phase velocity as the

VLF reflection height lowers. Examples of SPAs are shown in Fig.36a [15]. A book on the subject was produced by Mitra [67] summarising observations made up to 1973.

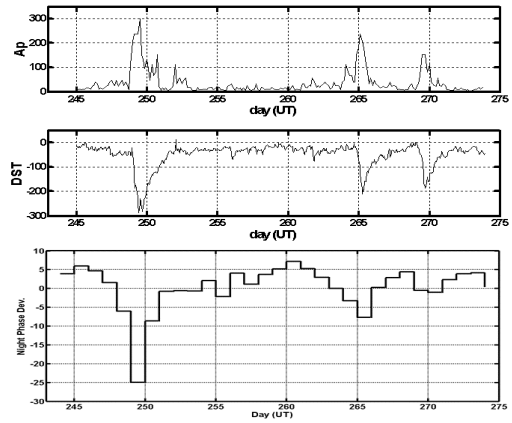


**Figure 35.** Three successive SPEs in 1982 observed on high latitude VLF southern hemisphere propagation paths and the associated geomagnetic disturbances.

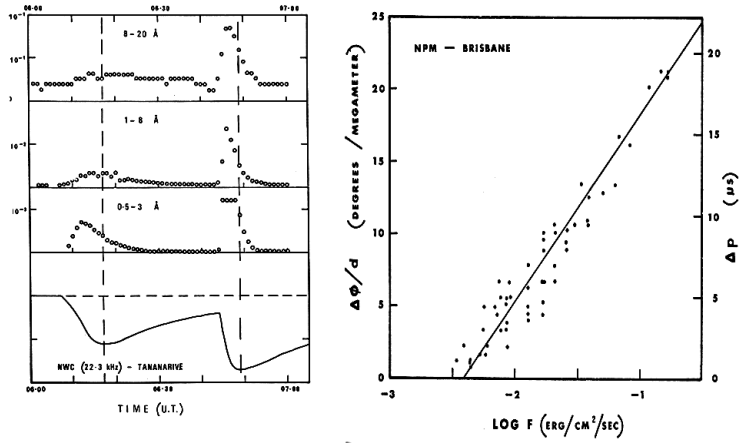


a b

**Figure 36**. a – The VLF phase response to two solar x-ray flares of differing characteristics b – linear relation between SPA magnitude and solar flare flux in the 1-8 angstrom range [15].

Fig.36a provides an example of solar flare flux for two successive solar flares with different UV and x-ray characteristics as seen by satellite along with the resultant VLF SPAs. Not all solar flares produce such strong UV and x-ray emission and they are perhaps best described as solar x-ray flares to distinguish them from the more common variety. Note that the SPA phase plots are inverted with respect to the format now usually used. The first solar flare peaks at successive times in the three solar UV/x-ray bands. In contrast, the second flare is impulsive and appears to peak at the same time in all flux bands with a rapid recovery compared to the slow recovery of the associated SPA. The conclusion from the second flare is that the 30-40 minute time constant of SPA recovery commonly observed is indeed that of the ionosphere rather than that of the ionizing solar radiation [15].

Figure 36a shows that for flares, which peak at successive times in different UV/x-ray wavelengths, it is always possible to find a flux band which matches the rise to the peak of the associated SPA. No such possible choice is available for impulsive flux bursts. A time delay of some 1-9 minutes was found for a large variety of SPA with a peak occurrence at 5 minutes [15]. A detailed examination of this delay can be found in [68]. A "sluggish" response between solar output and ionospheric response has been noted in a variety of circumstances and was originally so named by Appleton many years ago, from ionospheric measurements made at mid-day. A similar time lag was noted in [69] from eclipse observations.

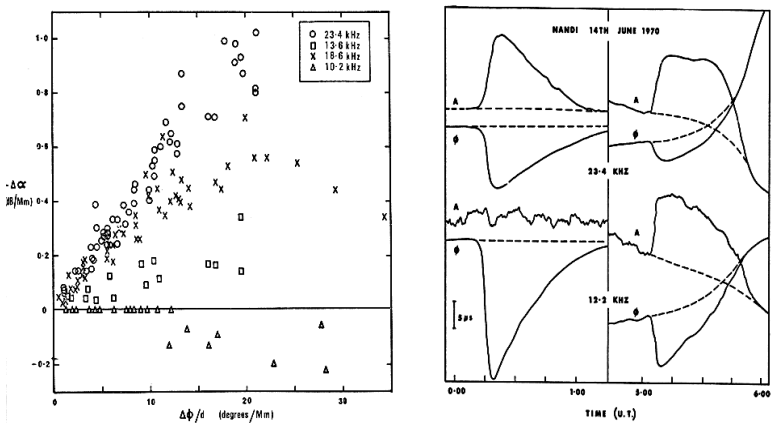


(a) (b)

**Figure 37**. a – Ratio of maximum signal amplitude deviation to maximum SPA deviation normalised for path length as measured at 4 frequencies over east to west paths received near Brisbane: b – comparison of SPAs at low and high zenith angle [15].

The maximum phase deviation of the SPA is linearly related to the log of the UV/x-ray flux peak as can be seen in Fig. 36b for NPM, Hawaii, received at Bribie Island, Australia

at 23.4 kHz [15] and in many other papers. The depression in reflection height has also been found to be a linear function of the log of solar fluence [70].

At low solar zenith angles (i.e., path mid-day) the SPA magnitudes measured were normalised by dividing by path length as was the peak change in signal strength. An increase in signal strength accompanied the SPA at frequencies above some 13 kHz. Below this frequency there could either be no change in signal strength or a decrease in signal strength (as typically seen at 10.2 kHz). Fig.37a shows the relationship between the SPA and the associated change in signal strength as seen near mid-day over the same path from Hawaii to Brisbane at 23.4 and 12.2 kHz and from NLK at 18.6 kHz to Brisbane on the same bearing. An interesting point here is that the signal increase on the long NPG-Brisbane path at 18.6 kHz seems to saturate and actually turn down for very high values of SPA, a point which needs independent verification if not due to changing zenith angle along the path. Such very large SPAs, are of course, rare.

Fig. 37b compares the relation between the associated SPA and signal change for similar solar events observed at a low solar zenith angle and at a high solar zenith angle (near path sunset). At the high solar zenith angle, the magnitude of the SPA is greatly reduced but the large increase in signal strength is still present at 23.4 kHz. At 12.2 kHz, there is now a large increase in signal amplitude at the high solar zenith angle whereas there was none for the mid-day solar event.

The solar zenith angle dependence of SPA phase and amplitude was characteristic as can be seen in Fig.38a for paths from NPM, Hawaii and Omega Hawaii to Deal, New Jersey and to Inubo, Japan, as received at 23.4 and 12.2 kHz. Here the normalised ratio of peak amplitude change to peak phase was shown to increase with increasing solar zenith angle [15]. Once again the change from signal reduction at 12.2 kHz to an increase at higher solar zenith angles is clear. Also note that there is a difference between the two paths which is particularly evident at the lower 12.2 kHz frequency where the ratio of amplitude to phase change is greater on the west to east path than on the east to west path.

Examination of the same SPAs on old VLF records over reciprocal paths between Omega transmitters would establish definitely whether this is indeed a true propagation non-reciprocity.

Further evidence for such non-reciprocity can be seen in Fig.38b for a series of SPAs observed over a west to east path between NAA (17.4 kHz) and Tananarive. This is a frequency where such SPAs would have been accompanied by a strong amplitude increase over the east to west paths shown in Fig.37a. Instead there is an increasingly negative amplitude effect over the NAA to Tananarive path with increasing SPA magnitude. There is clearly more work to be done on this question.

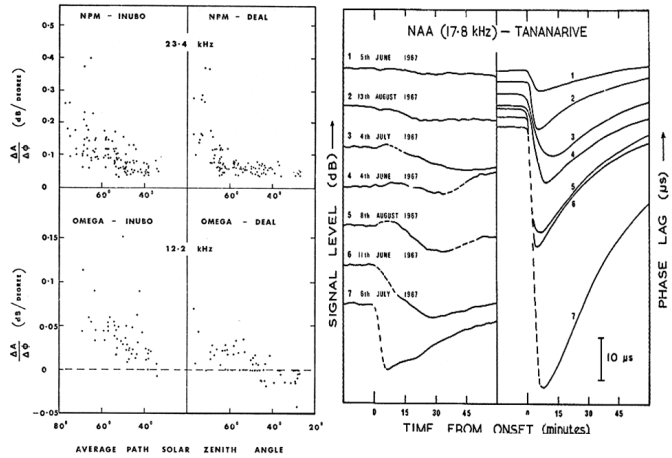


(a) (b)

**Figure 38.** a - The ratio of signal increase to SPA magnitude as a function of path solar zenith angle for transmissions from Hawaii on 23.4 and 12.2 kHz received in Japan and on the east coast of the U.S.A.: b – a series of SPAs of increasing magnitude accompanied by falls in signal level over the west to east path between NAA and Tananarive at 17.4 kHz [15].

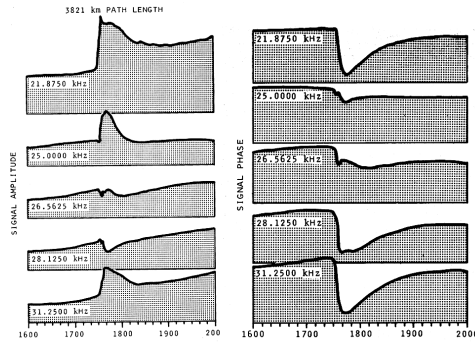


**Figure 39.** The effects of direct modal interference seen on the same SPA by a VLF sounder operating between Hawaii and California at a range of VLF frequencies [73].

Much effort has gone into characterising the effects of Solar x-ray flares on the β and h' exponential electron density model [71-72].

The paths discussed so far are ones in which only the first mode was significant when the path was entirely in daylight. Over shorter paths and at higher VLF frequencies, where at least two modes are significant at the receiver, modal interference will result in a rapid change in phase and amplitude characteristics for the same solar flare as seen at different VLF frequencies (and indeed over short paths of differing length at the same frequency). Fig. 39 provides an example obtained by a VLF sounder operating simultaneously at a number of VLF frequencies over the same path [73]. Here the changes in SPA phase and amplitude with frequency as the two or more mode vectors rotate with changing frequency is readily seen.

### 5.3 Solar eclipse

The effect of a solar eclipse on a VLF path results in a very characteristic decrease in phase velocity as the source of D region ionization produced by the normal sun decreases towards the night-time value and then recovers. Fig. 40b gives typical examples of such changes for the same solar eclipse crossing a number of VLF paths (Fig.40b) [69]. A theoretical

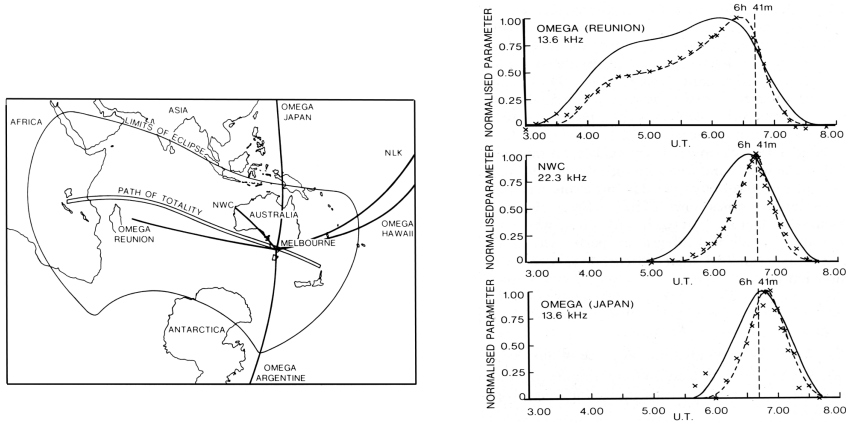


**Figure 40** a - A map of the path of totality and penumbra for the eclipse and VLF observing paths: b – Comparison of solar obscuration, calculated and observed time variation of the VLF eclipse effect on VLF phase over paths shown in Fig.40a [69].

calculation was found to match the time response of the VLF phase to the eclipse but the magnitude of the observed phase response was less than expected. In retrospect this discrepancy was caused by setting the edge of the sun at the photosphere. A greater radius should have been sought which would have reduced the apparent obscuration and established the effective height of the relevant UV solar emission.

As with SPAs, the phase and amplitude response for a solar eclipse is very repeatable on long VLF paths but becomes a complex function of distance and frequency over short multi-mode paths [72].

### 5.5 VLF as a geophysical detector

In more recent times, there has been a resurgence of VLF-based research where VLF paths are used as detectors of an increasing range of geophysical phenomenon. Such phenomena include high energy auroral precipitation, lightning-induced electron precipitation, electromagnetic and quasi-electrostatic coupling produced by lightning discharges (e.g., sprites and elves), cosmic gamma-ray bursts (GRBs) and g-ray flares from a magnetar, (see list with references in [75]). New receiving technology [76] allows the investigation of very short-lived phenomena and new theoretical approaches for calculating VLF fields have been developed [77]. As well, very short VLF paths are now being used to investigate localised phenomena, for example, long sought possible changes in ionospheric characteristics related to earthquakes [78].

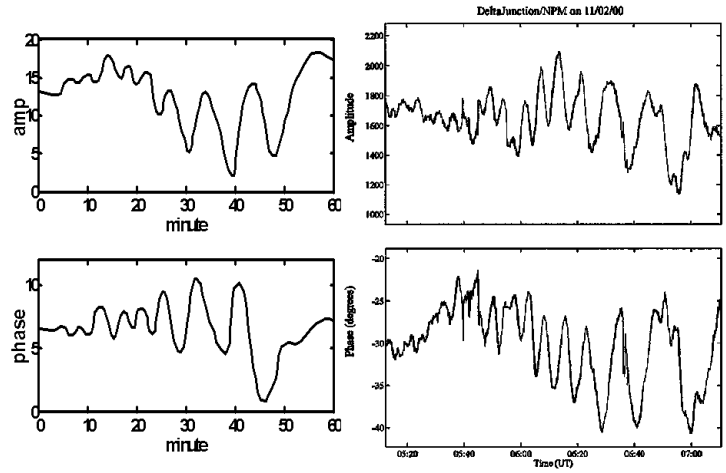


(a) (b)

**Figure 41.** Possible gravity waves detected at night on VLF paths with a component sensitive to the auroral zone a- Omega Australia to Adelaide (13.6 kHz): b – NPM received in Alaska (21.4 kHz) [79].

The possible effects of modal interference must be taken into account in interpreting geophysical results. Indeed over short VLF paths such effects are always present and the wave-hop theory can be a better theoretical approach to a situation where both phase and amplitude will vary rapidly with distance. The sensitivity to phase velocity change will be greatly enhanced for any VLF path where the receiver is close to a null in the direct

waveguide modal interference pattern or, for example, where the ground wave and first and/or higher order hops interfere on short paths.

There still remains one striking phenomena observed at VLF which has not as yet been published in the scientific literature or received the attention it deserves. Fig.41 shows examples of what appear to be gravity waves detected on VLF paths with a component in or near the auroral zone. Similar phenomena are well known as seen by airglow observations made at VLF reflection heights but no other method based on ionospheric reflection of radio waves seems to have produced the clarity seen in these VLF observations. The example in Fig.41a was obtained by the author over the path Omega Australia (13.6 kHz) to Adelaide. The example in Fig.41b was obtained over a path between NPM, Hawaii, and Delta Junction, Alaska [79].

## 6. CONCLUSION

The theory of VLF waveguide propagation is at a stage of maturity and thus can be used to interpret a large number of different geophysical phenomena observed on VLF paths. There remain problems in accounting for the extreme development of non-reciprocity for low latitude and trans-equatorial propagation at the magnetic equator and other possible minor effects elsewhere. No problem exists for eastward trans-equatorial propagation but for westward propagation, theoretical results continue to be limited because of the complexity of the calculations and the lack of sufficient experimental results for testing.

Short VLF paths are now in common use for geophysical measurements and are leading to a resurgence in the application of wave-hop theory.

## ACKNOWLEDGEMENTS

I am grateful to Prof. Sandip K. Chakrabarti for making this tutorial possible. I also extend my apologies to the many researchers in this field who have not been referenced.

## REFERENCES

1. R.L. Dowden, C.D.D. Adams, J.B. Brundell, P.E. Dowden. *J. of Atmospheric and Terrestrial Physics,* **56**, 1513 (1994).
2. E. R. Swanson., *IEEE, Proceeding,*. **71**, 1140 (1983).
3. T.B.Jones and K.Mowforth. *A Review of the Analytical Techniques for determining the Phase and Amplitude of a VLF Radio Wave Propagating in the Earth-Ionosphere Waveguide.* AGARD CONFERENCE PROCEEDINGS No. 305, Medium, Long and Very Long Wave Propagation (At frequencies less than 3000 kHz) (1982).
4. D.G. Morfitt. *Numerical comparison of the mode and the wave-hop theories of radiowave propagation at VLF and LF*", NELC Tech.Note TN2118 (1972 ).
5. R I. Barr, D. L. Jones, C. J. Rodger. *J. of Atmos and Solar-Terr. Phys*., **62,** 1689 (2000).
6. P. B. Morris, R. R. Gupta, R. S. Warren, P. M. Creamer. *Omega Navigation System Course Book, Volume 2*. ANALYTIC SCIENCES CORP READING MA, A949582, July 1994.

7. K. G. Budden, *The Wave-Guide Mode Theory of Wave Propagation: A Mathematical Treatment of the Propagation of Radio Waves at Great Distance Over Land and Through Water,* Logos Press-Elek Books and Ltd. Prentice-Hall (1961).
8. J.R.Wait. *Introduction to the Theory of VLF Propagation*, Proc. IRE, **50**, 1624 (1962).
9. J.R.Wait. *Electromagnetic waves in stratified media*, Pergamon Press, Oxford (1962).
10. J. Galejs. *Terrestrial Propagation of Long Electromagnetic Waves*. Pergamon Press, New York (1972).
11. R.A. Pappert. *Radio Sci*., **3**, 219 (1968).
12. J.R. Wait and K. P. Spies. "*Characteristics of the earth-ionosphere waveguide for VLF radio waves*, NBS Tech. Note 300 (1964).
13. J.R.Wait. *Advances in electronics and electron physics*, **25**, 145 (1968).
14. N. Thomson, M. A. Clilverd. *Journal of Atmospheric and Solar-Terrestrial Physics*, **62,** 601 (2000).
15. K. J. W. Lynn. PhD Thesis: *An Experimental Investigation of VLF Waveguide Propagation at Middle and Equatorial Latitudes*, University of Queensland, Brisbane (1973).
16. R.E. Schaal and S. Ananthakrishnan. *J. of Atmos. and Terr. Phys.,* **32**, 1831 (1970).
17. M.Yamashita. *J. of Atmos. and Terr. Phys*., **40**, 151 (1978).
18. S. Kumar, A. Kishore, V. Ramachandran. *Ann. Geophys.,* **26***,* 1451 (2008).
19. B. Burgess B. and T.B. Jones. *The Radio and Electronic Engineer*, **45**, 47 (1975).
20. V.E. Hildebrand, D.G. Morfitt. *An Evaluation of VLF Daytime Propagation Parameters using a Multi-frequency Sounder,* Naval Weapons Center, Corona Laboratories, California, NWCCL TP 759 (1968).
21. J. A. Ferguson. *Radio Science*, **30**, 775 (1995).
22. D.G. Morfitt and V.E. Hildebrand. Naval Weapons Center, Corona Laboratories, California, NWCCL TP 806 (1968).
23. P. Knight. *J. of Atmos. and Terr. Phys*. **34,** 401 (1972).
24. R.A. Smith, N.R. Coyne, R.G. Loch, I.A. Bourne. *Ground-based Radio Wave Propagation Studies of the Lower Ionosphere*, **1 and 2,** Defence Research Telecommunication Establishment, Ottawa, Canada (1967).
25. D.D. Crombie. *J. of Atmos. and Terr. Phys*., **12**, 110 (1958).
26. F.P. Snyder and R.A. Pappert. *Radio Sci*., **4**, 213 (1969).
27. R.J. Gallenberger and E.R. Swanson. *Variations in Omega propagation parameters* NELC/TR 1773 (1971).
28. D.G. Morfitt. *Effective electron density distributions describing VLF/LF data*, Naval Ocean Systems Center (NOSC), San Diego, TR 141 (1977).
29. R.A. Pappert and L.A. Hitney. *Radio Science,* **23,** 599 (1988).
30. K.J.W. Lynn. *Journal of Electrical and Electronic Engineering Aust*., **2**, 229 (1982).
31. J. E. Bickel, J. A. Ferguson, and G. V. Stanley. *Radio Science*, **5**, 19 (1970).
32. N.R.Thomson, M.Wayne, J.McRae. *J. of Geophysical Research (Space Physics)*, **114**, A08305, doi:10.1029/2008JA014001 (2009).
33. D.D.Crombie. *Radio Sci.*, **68D**, 27 (1964).
34. D. Walker. *Radio Sci.*, **69D**, 1435 (1965).
35. J.R. Wait. *J. of Geophys. Res*., **73**, 3537 (1968).
36. R. A. Pappert and D. G. Morfitt. *Radio Science,* **10,** 537.
37. K.J.W. Lynn. *J. of Atmos. and Terr. Phys*., **39,** 347 (1977).
38. S. Kumar. *Research Letters in Physics*, Article ID 216373, doi:10.1155/2009/216373 (2009).
39. G. Ries. *Radio Sci.*, **2**, 531 (1967).
40. F.K. Steele, D.D. Crombie. *Radio Science*, **2**, 547 (1967).
41. K.J.W.Lynn. *J. of Atmos. and Terr.Phys*., **35,** 439 (1973).
42. K.J.W. Lynn. *Radio Science,* **2,** 521 (1967).
43. T. Kikuchi. *J. Atmosph. Terrest. Phys*., **48**, 15 (1986).
44. A.B. Kaiser. *Radio Science,* **4,** 17 (1969).
45. K. Suzuki, K. Baba, T. Yoshioka, M.Kinoshita. *J.Geomag. Geoelectr.*, **25**, 403 (1973).
46. S.F. Mahmoud and J.C. Beal. Proc. IEE, **118**, 132 (1971).
47. A.B.Kaiser. *J. of Atmosp. and Terr.Phys*., **29,** 73 (1967).
48. A.B. Kaiser. *Radio Science,* **3,** 1084, (1968).
49. K.J.W. Lynn. *Radio Science,* **4,** 203 (1969).

50. L.A. Meara. *J .of Atmosph. and Terr.Phys*, **35**, 305 (1973).
51. F.P. Snyder. *Transequatorial propagation of VLF radio wave*, NOSC/TD- 431, Naval Ocean Systems Center, San Diego (1981).
52. C.P. Kugel. *Omega Near-Field Modal Interference Model Development: Data Supplement to NOSC TN 1237,* NOSC Technical Note TN-1259 (1983).
53. T. Kikuchi. *J. of Atmosph. and Terr.Phys*., **45**, 743 (1983).
54. C. Bianchi, L.Ciraolo. *Annali Di Geofisica*, **27**, 93 (1994).
55. K.J.W. Lynn. *J. of Atmosph. and Terr.Phys*., **37**, 1395 (1975).
56. K.J.W. Lynn. *Proc. of the 8th Annual Meeting of the International Omega Association*, Lisbon, Portugal (1983).
57. J. E. Bickel, J. A. Ferguson, and G. V. Stanley. *Radio Science*, **5**, 19 (1970).
58. F.P. Snyder. *Transequatorial propagation of VLF radio wave*, NOSC/TD- 431, Naval Ocean Systems Center, San Diego (1981).
59. K. Baba. *IEICE Transactions*, **E74,** 309 (1991).
60. M.V. Perel and O.L. Stesik. *Radio Science*, **32**, 199 (1997).
61. L.A. Pazynin. *Progress in Electromagnetic Research*, **6**, 75 (2009).
62. C. Z. Chilton and A. H. Diede. *J. of Geophysical Research,* **69,** 1319 (1964).
63. K.J.W. Lynn. *J. of Atmos.Terr.Phys.,* **40**, 145 (1978).
64. S. Westerlund, F.H. Reder, C.J. Abom. *Planetary & Space Sci*., **17**, 1329 (1969).
65. M. A. Clilverd, C. J. Rodger, T. U. Annika Seppälä, E. Turunen, A. Botman, N. R. Thomson. *J. of Geophysical Research,* **110,** AO9307 (2005).
66. A.P. Mitra, A. P. *Ionospheric Effects of Solar Flares*, Springer, New York, 1974.
67. V. Žigman, D.Grubor, D. Šulič. *J. of Atmos & Solar-Terr.Phys.***69**, 775 (2007).
68. K.J.W. Lynn. *J. of Atmos.Terr.Phys.***, 68,** 1309 (1981).
69. A.A. Pacini and J.P. Raulin. *J. Geophys. Res*., **111**, A09301, doi:10.1029/2006JA011613 (2006).
70. P. Kaufmann and A.M. Mendes. *J. of Geophysical Research,* **73,** 2487 (1968).
71. W.M. McRae and N.R. Thomson. *J. of Atmos & Solar-Terr.Phys.,* **66,** 77 (2004).
72. V.E. Hildebrand and D.G. Morfitt. *Examination of VLF/LF Propagation Effects as a Function of Frequency,* Naval Weapons Center, Corona Laboratories, California, NWCCL TP -886 (1969).
73. M.A. Clilverd, C.J. Rodger, N. R. Thomson, J. Lichtenberger, P. Steinbach, P. Canon, M.J. Angling. *Radio Science*, **36,** 773 (2001).
74. U. S. Inan, N. G. Lehtinen, R. C. Moore, K. Hurley, S. Boggs, D. M. Smith,G. J. Fishman. *Geophysical Research Letters*, **34**, L08103 (2007).
75. M.B. Cohen, U. S. Inan, W. Pascha. *IEEE Trans on Geoscience and Remote Sensing*, **48**, 3 (2010).
76. S.A. Cummer. *IEEE Trans. On Antennas and Propagation*, **48**, 1420 (2000).
77. M. Hayakawa*. Sensors*, 7, 1141 (2007).
78. M. Yoshida, T. Yamauchi, T. Horie, and M. Hayakawa. *Nat. Hazards Earth Syst. Sci.,* 8, 129–134, (2008).
79. T.F. Bell, U.S. Inan, M.K. Demirkol, M.W. Chevalier, R. Moore. *Very Low Frequency (VLF) Remote Sensing of Gravity Waves Generated by the Auroral Electrojet*, Final Technical Report, STAR Laboratory, Stanford University, California (2002).